Proceedings of the Korean Nuclear Society Spring Meeting
Cheju, Korea, May 2001

Coarse Mesh Diffusion Synthetic Acceleration of Bi-Linear Discontinuous Finite Element S_N Calculation in x-y Geometry

Kang-Seog Kim, Sung Quun Zee
Korea Atomic Energy Research Institute
P.O. Box 105, Yusung, Taejon, Korea 305-333

Todd S. Palmer
Department of Nuclear Engineering, Oregon State University, 100 Radiation Center, Corvallis, OR 97331-5903

Absract

We demonstrates that the diffusion equation discretized on a coarse mesh can be employed to accelerate the transport equation. Our results show that coarse mesh diffusion synthetic acceleration (DSA) in x-y geometry is very effective for thin and intermediate mesh spacings independent of the scattering ratio, but is not effective for purely scattering problems and high aspect ratio zoning. However, if the scattering ratio is less than about 0.95, this procedure is very effective for all mesh spacing. This procedure can be well applicable to reactor physics analysis problems in which the scattering ratio is always less than about 0.9.

I. INTRODUCTION

It has long been known that the success of a diffusion synthetic acceleration (DSA) scheme is very sensitive to the discretization of the transport and diffusion equations. “Inconsistent” discretizations or discretizations of the transport and diffusion equations which are not derived from one another have designed and proven effective,[1] but the degree of inconsistency which is effective is an open problem. Although inconsistencies in discretization have worked, all DSA schemes employed the same size in the high and low order equations. If it were possible to solve the diffusion equation on a mesh which has fewer zones than that used for the transport equation, the overall efficiency of the transport calculation should increase.

Anghel proposed coarse mesh diffusion acceleration for deterministic transport, but his research involved only diamond differencing in slab and x-y geometries. [2] Furthermore, no analyses were performed to quantify the effectiveness of this method in x-y geometry. While the purpose of his research was to develop the coarse mesh acceleration scheme for the transport calculation, no work was done to compare its behavior to that of standard fine mesh DSA.

In this research we demonstrate that the low order diffusion equation discretized on a coarse mesh can be employed to accelerate the fine mesh transport equation. We already showed that coarse mesh DSA in slab geometry is unconditionally stable and as rapidly convergent as fine mesh DSA. [2] Our results in x-y geometry show that coarse mesh DSA is as effective as conventional DSA for thin and intermediate mesh spacings, but not efficient for thick mesh spacings when the scattering ratio is unity. However, if the scattering ratio (c) is at least somewhat less than 1.0 ($c \leq 0.95$), coarse mesh DSA converges very fast for all mesh

spacings. We have used Adams and Martin's modified 4-step method (M4S)[1] to generate DSA equations for bilinear discontinuous (BLD) and fully lumped bilinear discontinuous (FLBLD) transport in x-y geometry. To verify the effectiveness of our procedure, we have also performed a Fourier analysis. We have implemented to corroborate the findings of our Fourier analysis for FLBLD M4S DSA schemes in x-y geometry. We use the multi-level technique[4,5] to solve the coarse mesh diffusion equation in x-y geometry. We find excellent agreement between our implementation and analysis results.

II. COARSE MESH DIFFUSION SYNTHETIC ACCELERATION

II.1 General Description

DSA schemes begin with source iteration (SI) for S_N transport equations:

$$\mathbf{L}_F \mathbf{Ø}_F^{(l+1/2)} = \mathbf{S}_F \mathbf{Ø}_F^{(l)} + \mathbf{Q}_F, \tag{1}$$

where $\mathbf{L}_F$ is a transport operator, $\mathbf{S}_F$ is a scattering operator, $\mathbf{Q}_F$ is an external source, and Y_F is an angular flux and subscript 'F' denotes the fine mesh and 'l' is the iteration index. Since SI is very slow in converging for very highly scattering ratio problems, diffusion synthetic acceleration (DSA) has been developed to accelerate the convergence of the iterative process. The next step in DSA is to calculate the residual, $\mathbf{R}_F$, as follows:

$$\mathbf{R}_F = \mathbf{Q}_F - (\mathbf{L}_F - \mathbf{S}_F)\mathbf{Ø}_F^{(l+1/2)} = \mathbf{S}_F(\mathbf{Ø}_F^{(l+1/2)} - \mathbf{Ø}_F^{(l)}), \tag{2}$$

This residual is used in diffusion calculation as a source. The low order diffusion equation on a fine mesh is

$$\mathbf{D}_F \mathbf{f}_F^{(l+1)} = \mathbf{R}_F, \tag{3}$$

where

$$\mathbf{f}_F^{(l+1)} = \mathbf{Ö}_F^{(l+1)} - \mathbf{Ö}_F^{(l+1/2)}, \tag{4}$$

and $\mathbf{D}_F$ is a diffusion operator. The final update of the scalar flux is

$$\mathbf{Ö}_F^{(l+1)} = \mathbf{Ö}_F^{(l+1/2)} + \mathbf{f}_F^{(l+1)}. \tag{5}$$

In our coarse mesh DSA method, the diffusion calculation is performed on a coarse mesh. Therefore, a restriction operation is needed for the residual on a fine mesh:

$$\mathbf{R}_C = \mathbf{I}_{F\to C}\mathbf{R}_F = \mathbf{I}_{F\to C}\mathbf{S}_F(\mathbf{Ø}_F^{(l+1/2)} - \mathbf{Ø}_F^{(l)}), \tag{6}$$

where $\mathbf{I}_{F\to C}$ is a restriction operator and subscript 'C' denotes the coarse mesh. In coarse mesh DSA, the low order diffusion equation is performed on a coarse mesh:

$$\mathbf{D}_C \mathbf{f}_C^{(l+1)} = \mathbf{R}_C, \tag{7}$$

where $\mathbf{D}_C$ is a diffusion operator on a coarse mesh.

The final step in coarse mesh DSA is the prolongation operation on the scalar flux correction:

$$\mathbf{f}_F = \mathbf{I}_{C\to F}\mathbf{f}_C, \tag{8}$$

where $\mathbf{I}_{C\to F}$ is a prolongation operator.

Our coarse mesh DSA procedure includes the following three stages:

a) A transport source iteration is performed on a fine mesh, and a restriction operation for scalar fluxes is followed.
b) A diffusion acceleration calculation is performed on a coarse mesh with interpolating prolongation.
c) A final prolongation is performed to get the correction terms on the fine mesh.

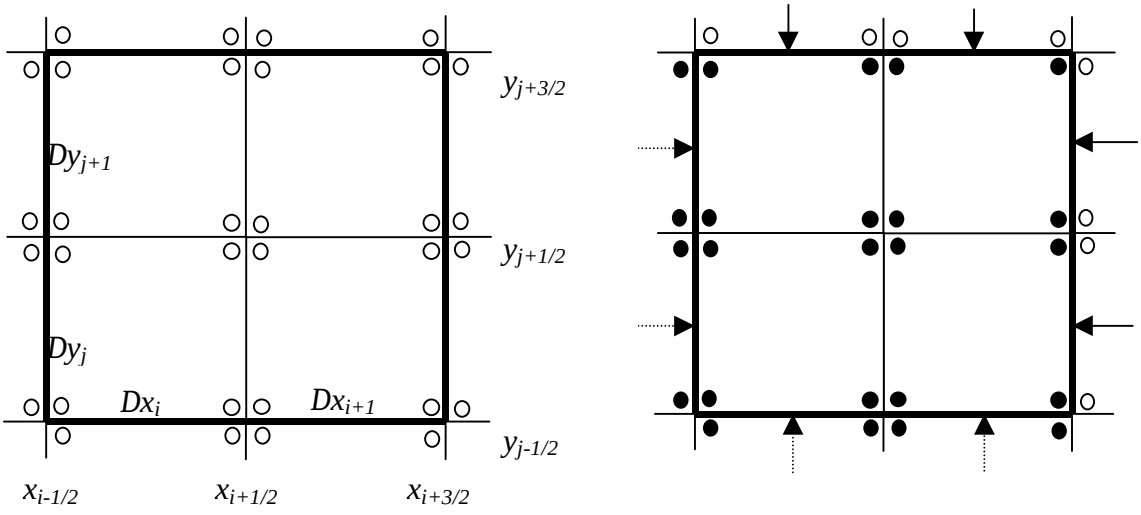

(a) Method-1 (b) Method-2

○ : From coarse-mesh iteration

● : From current fine-mesh iteration

Figure 1 Grids in BLD scheme and local prolongation operation methods

We used *spatial moment conservation* for the restriction operation, and we tried several methods for the prolongation operation.

All of the discretized equations used in our research are listed on the appendices. Fine mesh S_N transport equations, and coarse mesh diffusion acceleration equations are shown in Appendices A and B, respectively.

II.2 Restriction and Interpolating Operations

There are several restriction methods such as *injection*, *full weighting*[6] and *spatial moment conservation*[7]. The restriction operation of *injection* is such that the coarse mesh vector simply takes its value directly from the corresponding fine grid point. The *full weighting* restriction operation defines the values of the coarse grid vectors as a weighted average of values at neighboring fine grid points. We selected the *spatial moment conservation* method, [7] which has been proven to be the best in our calculations. The notation used to describe the fine and coarse mesh unknowns is shown in Figure 1. We consider only a coarsening of a factor of two: i.e. four fine mesh cells become a single coarse mesh cell in x-y geometry.

The *spatial moment conservation* restriction method for BLD in x-y geometry requires the specification of four basis functions shown in eqs. (A.10)~(A.13).

Using these four basis functions to calculate spatial moments of our scalar fluxes, the restriction operator ($\mathbf{I}_{F\rightarrow C}$) can be calculated to conserve the spatial moments between the coarse and fine meshes. For simplicity, we include the restriction operator for a constant mesh spacing for each direction. The restriction operation is as follows:

$$\begin{bmatrix} f_{k,l} \\ f^{x}_{k,l} \\ f^{y}_{k,l} \\ f^{xy}_{k,l} \end{bmatrix} = \begin{bmatrix} \frac{1}{4} & 0 & 0 & 0 & \frac{1}{4} & 0 & 0 & 0 & \frac{1}{4} & 0 & 0 & 0 & \frac{1}{4} & 0 & 0 & 0 \\ \frac{-3}{8} & \frac{1}{8} & 0 & 0 & \frac{3}{8} & \frac{1}{8} & 0 & 0 & \frac{-3}{8} & \frac{1}{8} & 0 & 0 & \frac{3}{8} & \frac{1}{8} & 0 & 0 \\ \frac{-3}{8} & 0 & \frac{1}{8} & 0 & \frac{-3}{8} & 0 & \frac{1}{8} & 0 & \frac{3}{8} & 0 & \frac{1}{8} & 0 & \frac{3}{8} & 0 & \frac{1}{8} & 0 \\ \frac{9}{16} & \frac{-3}{16} & \frac{-3}{16} & \frac{1}{16} & \frac{-9}{16} & \frac{-3}{16} & \frac{3}{16} & \frac{1}{16} & \frac{-9}{16} & \frac{3}{16} & \frac{-3}{16} & \frac{1}{16} & \frac{9}{16} & \frac{3}{16} & \frac{3}{16} & \frac{1}{16} \end{bmatrix} \begin{bmatrix} \mathbf{\ddot{O}}_{i,j} \\ \mathbf{\ddot{O}}_{i+1,j} \\ \mathbf{\ddot{O}}_{i,j+1} \\ \mathbf{\ddot{O}}_{i+1,j+1} \end{bmatrix}, \quad (9)$$

where

$$\mathbf{\ddot{O}}_{i,j} = \left(f_{i,j}, f^{x}_{i,j}, f^{y}_{i,j}, f^{xy}_{i,j} \right)^{T}. \quad (10)$$

The interpolating prolongation operator ($\mathbf{I}_{C\rightarrow F}$) in x-y geometry is used to interpolate the coarse mesh information to the fine mesh as follows:

$$\begin{bmatrix} f_{i,j} \\ f^{x}_{i,j} \\ f^{y}_{i,j} \\ f^{xy}_{i,j} \\ f_{i+1,j} \\ f^{x}_{i+1,j} \\ f^{y}_{i+1,j} \\ f^{xy}_{i+1,j} \\ f_{i,j+1} \\ f^{x}_{i,j+1} \\ f^{y}_{i,j+1} \\ f^{xy}_{i,j+1} \\ f_{i+1,j+1} \\ f_{i+1,j+1} \\ f_{i+1,j+1} \\ f_{i+1,j+1} \end{bmatrix} = \begin{bmatrix} 1 & -1/2 & -1/2 & 1/4 \\ 0 & 1/2 & 0 & -1/4 \\ 0 & 0 & 1/2 & -1/4 \\ 0 & 0 & 0 & 1/4 \\ 1 & 1/2 & 1/2 & -1/4 \\ 0 & 1/2 & 0 & -1/4 \\ 0 & 0 & 1/2 & 1/4 \\ 0 & 0 & 0 & 1/4 \\ 1 & -1/2 & 1/2 & -1/4 \\ 0 & 1/2 & 0 & 1/4 \\ 0 & 0 & 1/2 & -1/4 \\ 0 & 0 & 0 & 1/4 \\ 1 & 1/2 & 1/2 & 1/4 \\ 0 & 1/2 & 0 & 1/4 \\ 0 & 0 & 1/2 & 1/4 \\ 0 & 0 & 0 & 1/4 \end{bmatrix}_{16\times 4} \begin{bmatrix} f_{k,l} \\ f^{x}_{k,l} \\ f^{y}_{k,l} \\ f^{xy}_{k,l} \end{bmatrix}. \quad (11)$$

The form of the low order diffusion equation on the coarse mesh is exactly the same on the fine mesh. (Appendix B) The coarse mesh spacing is obtained by summing mesh spacings of two adjacent cells.

We have investigated several different prolongation methods to get the best results and introduce two methods here:

1. Method-1 includes SI for S_N transport equations with a restriction operation by eq. (9), and the final interpolating prolongation simply by eq. (11). (Figure 1 (a))
2. Method-2 includes method-1 and an additional prolongation operation updating inner unknowns in the local solve with incident flux from the neighboring local solve. (Figure 1 (b))

The additional prolongation operation includes the local solve for the sub-cells where the same diffusion acceleration equations in Appendix B are used with the incident information from the neighboring cells. We analyze these two methods to determine their convergence behavior using a Fourier analysis and confirm these results by implementing the techniques in a numerical transport code.

III. FOURIER ANALYSIS

The matrix of Fourier analysis for coarse mesh DSA method-1 is as follows:

$$w\mathbf{A} = \left[\mathbf{S} + \mathbf{I}_{\mathrm{C}\to\mathrm{F}}\mathbf{D}_{\mathrm{C}}^{-1}\mathbf{I}_{\mathrm{F}\to\mathrm{C}}(\mathbf{S}-\mathbf{I})\right]\mathbf{A}, \tag{12}$$

where w is a eigenvalue, $\mathbf{A}$ is a eigenvector, $\mathbf{S}$ is a matrix from SI, $\mathbf{D_c}$ is a matrix from diffusion acceleration equations in a coarse mesh and $\mathbf{I}$ is a identity matrix.

The matrix of Fourier analysis for coarse-mesh DSA method-2 is as follows:

$$w\mathbf{A} = \left[\mathbf{S} + \mathbf{D}_f'^{-1}\left(\mathbf{G}_f'\mathbf{I}_{\mathrm{C}\to\mathrm{F}}\mathbf{D}_c^{-1}\mathbf{I}_{\mathrm{F}\to\mathrm{C}} + \mathbf{I}\right)(\mathbf{S}-\mathbf{I})\right]\mathbf{A}, \tag{13}$$

where $\mathbf{D}\ell_{\mathrm{f}}$ and $\mathbf{G}\ell_{\mathrm{f}}$ are matrices from fine-mesh local diffusion equation with slightly different iteration indices due to the use of the most recently calculated data.

We have performed a Fourier analysis of coarse mesh M4S DSA with BLD and FLBLD in x-y geometry. The results of our Fourier analysis are shown in Tables 1~4. Fourier analysis was performed for the BLD and FLBLD M4S DSA with S_8 quadrature set and purely (c=1.0) and highly (c=0.95) scattering problems.

Table 1 shows the resulting spectral radii for the BLD M4S DSA scheme when the scattering ratio is unity. All two methods are unconditionally stable and convergent for thin and intermediate mesh spacings, but the spectral radius goes to unity as the mesh spacing and/or aspect ratio increases. The mesh spacing is less than 1.0 *mfp*, the simple coarse mesh DSA (method-1) can be used without any further prolongation, as in slab geometry. Method-2 is very efficient for the thin and intermediate mesh spacings (≤ 3.0 *mfp*), but the spectral radius increases as the mesh spacing and aspect ratio increases. This means that our coarse mesh DSA in x-y geometry is not effective for optically thick and diffusive problems. Table 2 shows the analytic spectral radii of coarse mesh DSA with BLD when the scattering ratio is 0.95. Method-1 has the same trend as the purely scattering problem (c=1.0), but the results of method-2 are completely different. The spectral radius goes to zero as the mesh spacing increases, but the results still degrade for the high aspect ratio problems. However, if the aspect ratio is less than 100, method-2 will be very effective and rapidly convergent.

Tables 3 and 4 show the analytic spectral radii of FLBLD coarse mesh DSA when the scattering ratio is unity and 0.95. The results are almost the same as those from BLD coarse mesh DSA.

Table 1. Fourier analysis results for coarse mesh BLD M4S DSA (c=1.0, S_8)

$\sigma_t\Delta x$	$\sigma_t\Delta y$					
	0.01	0.1	1.0	3.0	10.0	100.0
0.01	0.22 0.22					Method 1 Method 2
0.1	0.22 0.22	0.20 0.22				
1.0	0.47 0.36	0.47 0.35	0.47 0.44			
3.0	0.81 0.64	0.81 0.62	0.81 0.47	0.81 0.46		
10.0	0.97 0.93	0.97 0.93	0.97 0.84	0.97 0.73	0.97 0.64	
100.0	1.00 1.00	1.00 1.00	1.00 1.00	1.00 0.99	1.00 0.98	1.00 0.95

Table 2. Fourier analysis results for coarse mesh BLD M4S DSA (c=0.95, S_8)

s_tDx	s_tDy					
	0.01	0.1	1.0	3.0	10.0	100.0
0.01	0.20 0.21					Method 1 Method 2
0.1	0.20 0.21	0.19 0.20				
1.0	0.45 0.34	0.45 0.33	0.45 0.40			
3.0	0.76 0.58	0.76 0.55	0.76 0.42	0.76 0.38		
10.0	0.92 0.83	0.92 0.81	0.92 0.62	0.92 0.48	0.92 0.41	
100.0	0.95 0.89	0.95 0.87	0.95 0.69	0.95 0.49	0.95 0.36	0.95 0.10

Table 3. Fourier analysis results for coarse mesh FLBLD M4S DSA (c=1.0, S_8)

$\sigma_t\Delta x$	$\sigma_t\Delta y$					
	0.01	0.1	1.0	3.0	10.0	100.0
0.01	0.22 0.23					Method-1 Method-2
0.1	0.22 0.24	0.23 0.25				
1.0	0.70 0.54	0.70 0.53	0.70 0.48			
3.0	0.96 0.82	0.96 0.81	0.96 0.63	0.96 0.53		
10.0	1.02 0.97	1.02 0.97	1.02 0.92	1.02 0.85	1.02 0.82	
100.0	1.00 1.00	1.00 1.00	1.00 1.00	1.00 1.00	1.02 0.99	1.00 0.98

Table 4. Fourier analysis results for coarse mesh FLBLD M4S DSA (c=0.95, S_8)

$\sigma_t\Delta x$	$\sigma_t\Delta y$					
	0.01	0.1	1.0	3.0	10.0	100.0
0.01	0.21 0.21					Method 1 Method 2
0.1	0.21 0.22	0.22 0.23				
1.0	0.66 0.50	0.66 0.49	0.66 0.44			
3.0	0.87 0.74	0.87 0.72	0.87 0.51	0.87 0.41		
10.0	0.94 0.87	0.94 0.85	0.94 0.66	0.94 0.47	0.94 0.32	
100.0	0.95 0.89	0.95 0.88	0.95 0.69	0.95 0.47	0.95 0.25	0.95 0.04

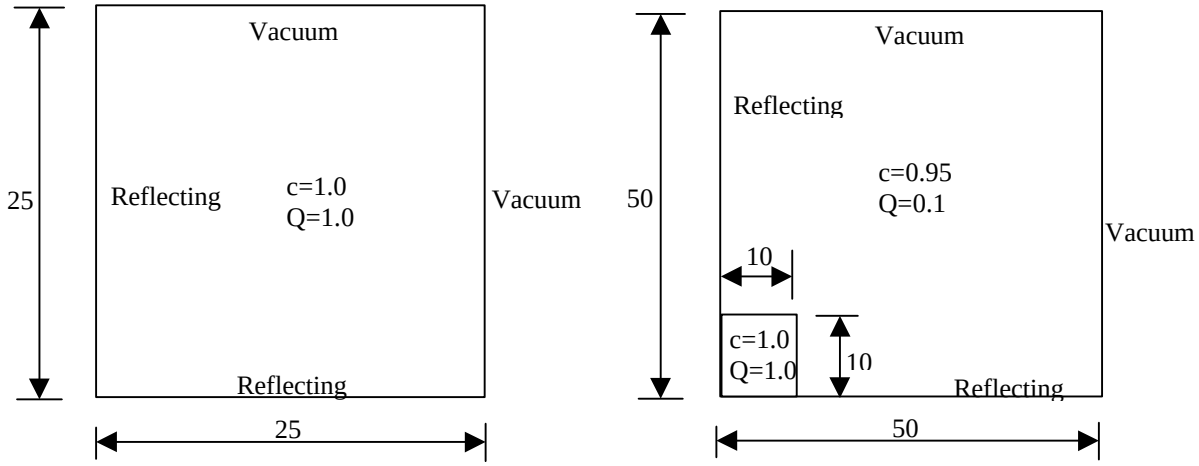

Figure 2 Geometry for numerical test problems

The high spectral radius for thick mesh spacings and purely scattering problems is likely due to the quality of the incident fluxes at the interface obtained from the interpolating prolongation. This information does not contain enough physics to work well with the local fine mesh diffusion calculation. Since the spectral radius decreases significantly with small amount of absorption for the thick mesh spacing, the high spectral radius problem can be solved by improving the incident flux information at the interface. This problem will be addressed in future work.

IV COMPUTATIONAL RESULTS

We have implemented our methods in a transport code to see the behavior of the spectral radii and to compare those with the theoretical spectral radii.

We performed model problem calculations only for the coarse mesh FLBLD M4S DSA methods in x-y geometry, using the multi-level technique[4,5] to solve the coarse mesh FLBLD diffusion equation. The model problems are identical to the model problems in Reference 4 , which are shown in Figure 2. We slightly modified the model problem for our purpose in the following manners.

Problem # 1 (Figure 1 (a)) is a homogeneous region with isotropic scattering, a scattering ratio of unity and 0.95, and a constant isotropic distributed source. The rectangle has reflective boundaries on the bottom and left sides and vacuum boundaries on the right and top sides. There are 24 cells along the *x*-axis and 24 cells along the *y*-axis. All of the calculations were performed with S_8 quadrature set.

Problem # 2 (Figure 1 (a)) shows the overall efficiency of our procedure as a function of scattering ratio. The geometry is identical to that of the first model problem. We fix the *x*- and *y*-mesh spacing at 1.0 *mfp*. The scattering ratio is varied from 1.0 to 0.1, and each calculation is performed once without acceleration and once with acceleration.

Problem # 3 (Figure 1 (b)) demonstrates the effectiveness of the method for inhomogeneous source problems. It consists of a rectangular region that is 50 cm in length and width with an inner region 10 cm in length and width. The rectangle has reflective boundaries on the bottom and left sides and vacuum boundaries on the top and right sides.

Both the inner and outer regions have a total cross section of 1.0 cm^{-1} and a scattering ratio of 0.95. The inner region has a source of 1.0 while the outer region has a source of 0.1. The number of spatial cells varies between calculations. All of the calculations in this model problem were performed with S_8 quadrature set.

The results for Problem # 1 with the scattering ratio of 1.0 and 0.95 are shown in Table 5. Since the multi-level method is used to solve the coarse mesh diffusion equation, the observed spectral radii can be slightly greater than the analytic spectral radii, due to the insufficient convergence in the asymptotic or FLBLD diffusion equations. For thin mesh spacing problems, the observed spectral radii are sometimes much less than the analytic spectral radii because of the large amount of leakage. However, the observed spectral radii correspond well with the analytical spectral radii. When the scattering ratio is 0.95, the coarse mesh DSA with method-2 is rapidly convergent for any mesh spacing. Since the typical neutronic problems include highly scattering media but not purely scattering media, this procedure can be applied to most practical neutronic analyses and will accelerate the transport calculation with less computational time spent in the diffusion calculation.

Table 6 shows the observed spectral radii from Problem # 2 for the various scattering ratios. Since the mesh spacing is set to 1.0 *mfp*, all three methods are rapidly convergent for all scattering ratios.

Table 7 shows how coarse mesh DSA works in mildly inhomogeneous source problems with the scattering ratio of 0.95. The results show that coarse mesh DSA is rapidly convergent for the inhomogeneous problem. We did not consider the inhomogeneous problem where fine mesh cells with different material properties are collapsed into a homogeneous coarse mesh cell. In that case the volume-flux averaged cross sections must be incorporated to obtain reasonable results. In this research we have used the volume averaged cross sections.

Table 5. Spectral radii (number of iterations) for Problem # 1 (FLBLD, S_8, c=1.0)

Δx (mfp)	Δy (mfp)	c=1.0		c=0.95	
		Method-1	Method-2	Iterations	Spectral Radius
0.01	0.01	0.09(6)	0.10 (6)	0.09 (5)	0.09 (6)
0.01	0.1	0.14 (6)	0.14 (6)	0.13 (6)	0.13 (6)
0.01	1.0	0.30 (7)	0.17 (6)	0.25 (6)	0.17 (6)
0.01	3.0	0.30 (6)	0.18 (6)	0.24 (6)	0.17 (6)
0.01	10.0	0.23 (6)	0.14 (6)	0.23 (6)	0.13 (6)
0.01	100.0	0.11 (6)	0.11 (6)	0.10 (5)	0.11 (6)
0.1	0.1	0.25 (8)	0.27 (8)	0.23 (7)	0.25 (8)
0.1	1.0	0.66 (13)	0.50 (9)	0.63 (12)	0.45 (8)
0.1	3.0	0.85 (>15)	0.67 (15)	0.80 (>15)	0.59 (12)
0.1	10.0	0.90 (>15)	0.78 (>15)	0.86 (>15)	0.69 (13)
0.1	100.0	0.50 (7)	0.37 (7)	0.51 (6)	0.45 (6)
1.0	1.0	0.67 (14)	0.44 (8)	0.67 (13)	0.40 (7)
1.0	3.0	0.90 (>15)	0.53 (14)	0.86 (>15)	0.47 (9)
1.0	10.0	0.84 (>15)	0.85 (>15)	0.93 (>15)	0.61 (12)
1.0	100.0	0.98 (>15)	0.98 (>15)	0.89 (13)	0.66 (7)
3.0	3.0	0.90 (>15)	0.52 (11)	0.87 (>15)	0.36 (7)

Table 6. Results for Problem # 2 (FLBLD, S_8)

Scattering Ratio	Unaccelerated	Method-1	Method-2
1.0	1078	14	8
0.9	67	12	7
0.8	36	10	6
0.7	24	8	5
0.6	18	7	5
0.5	14	6	4
0.4	11	5	4
0.3	9	5	4
0.2	7	4	4
0.1	5	4	3

Table 7. Results for Problem # 3 (FLBLD, S_8, c=0.95)

Mesh Size	Δx=Δy (mfp)	Method-1		Method-2	
		Iterations	Spectral Radius	Iterations	Spectral Radius
10×10	5.00	>20	0.86	7	0.30
20×20	2.50	>20	0.80	7	0.37
30×30	1.67	16	0.73	7	0.39
40×40	1.25	14	0.71	7	0.41
50×50	1.00	12	0.61	7	0.41
60×60	0.83	10	0.56	7	0.41
70×70	0.71	9	0.52	7	0.38
80×80	0.63	9	0.48	7	0.35
90×90	0.56	9	0.45	7	0.28
100×100	0.50	8	0.42	7	0.26
120×120	0.42	8	0.38	7	0.27
140×140	0.36	7	0.34	7	0.26
160×160	0.31	7	0.31	7	0.25
180×180	0.28	7	0.27	7	0.23
200×200	0.25	7	0.26	7	0.23

IV. DISCUSSION AND CONCLUSION

We presented that the low order diffusion equation on a coarse mesh could be employed to accelerate the transport equation for advanced discretization schemes. Our procedure includes three steps: SI for S_N transport calculation, the solution for the coarse mesh diffusion equation and the linearly interpolating and the fine mesh local prolongation. We applied this procedure to the BLD and FLBLD DSA schemes in x-y geometry. We performed Fourier analysis to predict the analytic spectral radius and compared those with the observed spectral radius. We used the multi-level technique to solve the coarse mesh diffusion equations in x-y geometries, respectively.

The results in x-y geometry showed that coarse mesh DSA is as effective as conventional DSA for thin and intermediate mesh spacings, but not efficient for thick mesh spacings when the scattering ratio is unity. When the scattering ratio is less than 1.0 ($c \leq 0.95$),

coarse mesh DSA converges as fast as fine mesh DSA for all mesh spacings. As the scattering ratio decreases for the thick mesh spacing, the spectral radius decreases drastically. We note that this procedure will be very effective for most practical neutronic reactor analysis problems, because most of this type of problems do not include purely scattering media.

APPENDIX A
BLD/FLBLD S_N EQUATIONS IN X-Y GEOMETRY

In x-y geometry, the S_N transport equation is as follows:

$$\begin{aligned} m_m \frac{\partial}{\partial x}\psi_m(x,y) + h_m \frac{\partial}{\partial y}\psi_m(x,y) + \sigma_t(x,y)\psi_m(x,y) \\ = \frac{\sigma_s f(x,y)}{2\pi} + \frac{q(x,y)}{2\pi}, \quad m = 1,\ldots,M \end{aligned}, \tag{A.1}$$

where the number of discrete directions in the chosen quadrature set is M, and the scalar flux is defined in terms of the quadrature sum:

$$f(x,y) = \sum_{m=1}^{M} w_m \psi_m(x,y), \quad M = \frac{N(N+2)}{2}. \tag{A.2}$$

The quadrature weights, w_m, are normalized in the following manner:

$$\sum_{m=1}^{M} w_m = 2\pi . \tag{A.3}$$

The linear representations for the cell-average flux and cell-edge fluxes on the four faces of the cell are given by the following equations.

$$\psi_m(x,y) = \psi_{m,i,j} + \frac{2(x-x_i)}{\Delta x_i}\psi^x_{m,i,j} + \frac{2(y-y_j)}{\Delta y_j}\psi^y_{m,i,j} + \frac{2(x-x_i)}{\Delta x_i}\frac{2(y-y_j)}{\Delta y_j}\psi^{xy}_{m,i,j}, \tag{A.4}$$

$$\psi_m(x_{i-1/2},y) = \psi_{m,i-1/2,j} + \frac{2}{\Delta y_j}(y-y_j)\psi^y_{m,i-1/2,j}, \tag{A.5}$$

$$\psi_m(x,y_{j-1/2}) = \psi_{m,i,j-1/2} + \frac{2}{\Delta x_i}(x-x_i)\psi^x_{m,i,j-1/2}, \tag{A.6}$$

$$\psi_m(x_{i+1/2},y) = \psi_{m,i+1/2,j} + \frac{2}{\Delta y_j}(y-y_j)\psi^y_{m,i+1/2,j}, \tag{A.7}$$

$$\psi_m(x,y_{j+1/2}) = \psi_{m,i,j+1/2} + \frac{2}{\Delta x_i}(x-x_i)\psi^x_{m,i,j+1/2}. \tag{A.8}$$

There are eight unknowns in these representations: the cell-average flux (ψ_{ij}), two cell interior slopes ($\psi^x_{i,j}$, $\psi^y_{i,j}$ and $\psi^{xy}_{i,j}$), two exiting cell-edge fluxes ($\psi_{i+1/2,j}$ and $\psi_{i,j+1/2}$) and two exiting cell-edge slopes ($\psi^x_{i+1/2,j}$ and $\psi^y_{i,j+1/2}$). Therefore, four more equations are needed and can be generated by integrating the transport equation multiplied by four different weight functions:

$$\int_i dx \int_j dy\, b_k(x,y)[eq.(A.1)], \tag{A.9}$$

where

$$b_1(x,y) = 1.0, \tag{A.10}$$

$$b_2(x,y)=\frac{2}{\Delta x_i}(x-x_i), \tag{A.11}$$

$$b_3(x,y)=\frac{2}{\Delta y_j}(y-y_j), \tag{A.12}$$

$$b_4(x,y)=\frac{2}{\Delta x_i}(x-x_i)\frac{2}{\Delta y_j}(y-y_j). \tag{A.13}$$

The resulting equations are

$$\begin{aligned}&\frac{\mu_m}{\Delta x_i}(\psi_{m,i+1/2,j}-\psi_{m,i-1/2,j})+\frac{\eta_m}{\Delta y_j}(\psi_{m,i,j+1/2}-\psi_{m,i,j-1/2})+\sigma_{t,i,j}\psi_{m,i,j}\\&=\frac{\sigma_{s,i,j}}{2\pi}\phi_{i,j}+\frac{1}{2\pi}q_{i,j}\end{aligned}, \tag{A.14}$$

$$\begin{aligned}&\frac{\theta_{i,j}\mu_m}{\Delta x_i}(\psi_{m,i+1/2,j}+\psi_{m,i-1/2,j}-2\psi_{m,i,j})+\frac{\theta_{i,j}\eta_m}{\Delta y_j}(\psi^x_{m,i,j+1/2}-\psi^x_{m,i,j-1/2})\\&+\sigma_{t,i,j}\psi^x_{m,i,j}=\frac{\sigma_{s,i,j}}{2\pi}\phi^x_{i,j}+\frac{1}{2\pi}q^x_{i,j}\end{aligned}, \tag{A.15}$$

$$\begin{aligned}&\frac{q_{i,j}m_m}{\Delta x_i}(y^{\,y}_{m,i+1/2,j}-y^{\,y}_{m,i-1/2,j})+\frac{q_{i,j}h_m}{\Delta y_j}(y_{m,i,j+1/2}+y_{m,i,j-1/2}-2y_{m,i,j})\\&+s_{t,i,j}y^{\,y}_{m,i,j}=\frac{s_{s,i,j}}{2p}f^{\,y}_{i,j}+\frac{1}{2p}q^{y}_{i,j}\end{aligned}, \tag{A.16}$$

$$\begin{aligned}&\frac{q_{i,j}m_m}{\Delta x_i}(y^{\,y}_{m,i+1/2,j}+y^{\,y}_{m,i-1/2,j}-2y^{\,y}_{m,i,j})+\frac{q_{i,j}h_m}{\Delta y_j}(y^{\,x}_{m,i,j+1/2}+y^{\,x}_{m,i,j-1/2}-2y^{\,x}_{m,i,j})\\&+s_{t,i,j}y^{\,xy}_{m,i,j}=\frac{s_{s,i,j}}{2p}f^{\,xy}_{i,j}+\frac{1}{2p}q^{xy}_{i,j}\end{aligned}. \tag{A.17}$$

The four closure equations are as follows:

$$y^{\,x}_{m,i,j}=\left(\frac{l_x+1}{2}\right)y_{m,i+1/2,j}+\left(\frac{l_x-1}{2}\right)y_{m,i-1/2,j}-l_x y_{m,i,j},\qquad l_x=\frac{m_m}{|m_m|}, \tag{A.18}$$

$$y^{\,y}_{m,i,j}=\left(\frac{l_y+1}{2}\right)y_{m,i,j+1/2}+\left(\frac{l_y-1}{2}\right)y_{m,i,j-1/2}-l_y y_{m,i,j},\qquad l_x=\frac{h_m}{|h_m|}, \tag{A.19}$$

$$y^{\,xy}_{m,i,j}=\left(\frac{l_x+1}{2}\right)y^{\,y}_{m,i+1/2,j}+\left(\frac{l_x-1}{2}\right)y^{\,y}_{m,i-1/2,j}-l_x y^{\,y}_{m,i,j},\qquad l_x=\frac{m_m}{|m_m|}, \tag{A.20}$$

$$y^{\,xy}_{m,i,j}=\left(\frac{l_y+1}{2}\right)y^{\,x}_{m,i,j+1/2}+\left(\frac{l_y-1}{2}\right)y^{\,x}_{m,i,j-1/2}-l_y y^{\,x}_{m,i,j},\qquad l_x=\frac{h_m}{|h_m|}. \tag{A.21}$$

Here, $q_{i,j}$=3 are for the BLD scheme, $q_{i,j}$=1 for the FLBLD scheme.

APPENDIX B
DIFFUSION ACCELERATION EQUATION ON COARSE MESH

The low order diffusion equations on the coarse mesh are as follows:

$$\begin{aligned}\Delta y_l\left(g_{k+1/2,l}^{(l+2/3)}-g_{k-1/2,l}^{(l+2/3)}\right)+\Delta x_k\left(g_{k,l+1/2}^{(l+2/3)}-g_{k,l-1/2}^{(l+2/3)}\right)+\Delta x_k\Delta y_l s_{a,k,l}\,f_{k,l}^{(l+2/3)}\\ =\Delta x_k\Delta y_l s_{s0,k,l}(f_{k,l}^{(l+1/3)}-f_{k,l}^{(l)})\end{aligned}, \tag{B.1}$$

$$\begin{aligned}q_{k,l}\Delta y_l\left(g_{k+1/2,l}^{(l+2/3)}+g_{k-1/2,l}^{(l+2/3)}-2g_{k,l}^{m(l+2/3)}\right)+\Delta x_k\left(g_{k,l+1/2}^{x(l+2/3)}-g_{k,l-1/2}^{x(l+2/3)}\right)\\ +\Delta x_k\Delta y_l s_{a,k,l}\,f_{k,l}^{x(l+2/3)}=\Delta x_k\Delta y_l s_{s0,k,l}(f_{k,l}^{x(l+1/3)}-f_{k,l}^{x(l)})\end{aligned}, \tag{B.2}$$

$$\begin{aligned}\Delta y_l\left(g_{k+1/2,l}^{y(l+2/3)}-g_{k-1/2,l}^{y(l+2/3)}\right)+q_{k,l}\Delta x_k\left(g_{k,l+1/2}^{(l+2/3)}+g_{k,l-1/2}^{(l+2/3)}-2g_{k,l}^{h(l+2/3)}\right)\\ +\Delta x_k\Delta y_l s_{a,k,l}\,f_{k,l}^{y(l+2/3)}=\Delta x_k\Delta y_l s_{s0,k,l}(f_{k,l}^{y(l+1/3)}-f_{k,l}^{y(l)})\end{aligned}, \tag{B.3}$$

$$\begin{aligned}q_{k,l}\Delta y_l\left(g_{k+1/2,l}^{y(l+2/3)}+g_{k-1/2,l}^{y(l+2/3)}-2g_{k,l}^{m,y(l+2/3)}\right)+q_{k,l}\Delta x_k\left(g_{k,l+1/2}^{x(l+2/3)}+g_{k,l-1/2}^{x(l+2/3)}-2g_{k,l}^{h,x(l+2/3)}\right)\\ +\Delta x_k\Delta y_l s_{a,k,l}\,f_{k,l}^{xy(l+2/3)}=\Delta x_k\Delta y_l s_{s0,k,l}(f_{k,l}^{xy(l+1/3)}-f_{k,l}^{xy(l)})\end{aligned}, \tag{B.4}$$

where

$$s_{k,l}=\frac{\Delta x_i\Delta y_j s_{i,j}+\Delta x_{i+1}\Delta y_j s_{i+1,j}+\Delta x_i\Delta y_{j+1}s_{i,j+1}+\Delta x_{i+1}\Delta y_{j+1}s_{i+1,j+1}}{\Delta x_k\Delta y_l}, \tag{B.5}$$

and $f_{k,l}^{(l+1/3)}$ and $f_{k,l}^{(l)}$ are from eq. (16).

The current equations can be derived from the 1st ($\Sigma w_m h_m$· and $\Sigma w_m m_m$·) angular moments as follows:

$$\begin{aligned}g_{k+1/2,l}&=g_{k+1/2,l}^{+}+g_{k+1/2,l}^{-}\\ &=[a(f_{k,l}+f_{k,l}^{x})-\frac{D_{k,l}}{\Delta x_k}f_{k,l}^{x}]-[a(f_{k+1,l}-f_{k+1,l}^{x})+\frac{D_{k+1,l}}{\Delta x_{k+1}}f_{k+1,l}^{x}]\end{aligned}, \tag{B.6}$$

$$\begin{aligned}g_{k+1/2,l}^{y}&=g_{k+1/2,l}^{y+}+g_{k+1/2,l}^{y-}\\ &=[a(f_{k,l}^{y}+f_{k,l}^{xy})-\frac{D_{k,l}}{\Delta x_k}f_{k,l}^{xy}]-[a(f_{k+1,l}^{y}-f_{k+1,l}^{xy})+\frac{D_{k+1,l}}{\Delta x_{k+1}}f_{k+1,l}^{xy}]\end{aligned}, \tag{B.7}$$

$$\begin{aligned}g_{k,l+1/2}&=g_{k,l+1/2}^{+}+g_{k,l+1/2}^{-}\\ &=[a(f_{k,l}+f_{k,l}^{y})-\frac{D_{k,l}}{\Delta y_l}f_{k,l}^{y}]-[a(f_{k,l+1}-f_{k,l+1}^{y})+\frac{D_{k,l+1}}{\Delta y_{l+1}}f_{k,l+1}^{y}]\end{aligned}, \tag{B.8}$$

$$\begin{aligned}g_{k,l+1/2}^{x}&=g_{k,l+1/2}^{x+}+g_{k,l+1/2}^{x-}\\ &=[a(f_{k,l}^{x}+f_{k,l}^{xy})-\frac{D_{k,l}}{\Delta y_l}f_{k,l}^{xy}]-[a(f_{k,l+1}^{x}-f_{k,l+1}^{xy})+\frac{D_{k,l+1}}{\Delta y_{l+1}}f_{k,l+1}^{xy}]\end{aligned}, \tag{B.9}$$

$$g_{k,l}^{m}=-\frac{2D_{k,l}}{\Delta x_k}f_{k,l}^{x}, \tag{B.10}$$

$$g_{k,l}^{h}=-\frac{2D_{k,l}}{\Delta y_l}f_{k,l}^{y}, \tag{B.11}$$

$$g_{k,l}^{m,y}=-\frac{2D_{k,l}}{\Delta x_k}f_{k,l}^{xy}, \tag{B.12}$$

$$g_{k,l}^{m,x} = -\frac{2D_{k,l}}{\Delta y_l} f_{k,l}^{xy} . \qquad \text{(B.13)}$$

The boundary conditions are that the incident partial current is zero for vacuum or incident boundaries, and the net current is zero for reflecting boundaries.

REFERENCES

1. M. L. Adams and W. R. Martin, “Diffusion Synthetic Acceleration of Discontinuous Finite Element Transport Iterations,” *Nucl. Sci. Eng.*, **111**, 145-167 (1992)
2. V. N. P. Anghel, “Coarse-mesh Diffusion Acceleration Technique for Transport Calculation,” *Nucl. Sci. Eng.*, **97**, 249-256 (1987)
3. K. S. Kim, Todd S. Palmer, "Coarse-Mesh Diffusion Synthetic Acceleration in Slab Geometry," *Trans. Am. Nucl. Soc.*, **76** (2000)
4. J. E. Morel and J. E. Dendy, Jr. and T. A. Wareing, “Diffusion-Accelerated Solution of theTwo-Dimensional S_N Equations with Bilinear-Discontinuous Differencing,” *Nucl. Sci. Eng.*, **115**, 304-319 (1993)
5. K. S. Kim and T. S. Palmer, “Multi-level Techniques for the Solution of Discontinuous Diffusion Acceleration Equations in x-y Geometry," (In review)
6. W. L. Briggs, “A Multigrid Tutorial,” Society for Industrial and Applied Mathematics (1987)
7. A. Barnett, J. E. Morel and D. R. Harris, “A Multigrid Acceleration Method for the One-Dimensional S_N Equations with Anisotropic Scattering,” *Nucl. Sci. Eng.*, **102**, 1-21 (1989)